

Spontaneous fractional Chern insulators in transition metal dichalcogenides Moiré superlattices

Heqiu Li,¹ Umesh Kumar,² Kai Sun,¹ and Shi-Zeng Lin³

¹*Department of Physics, University of Michigan, Ann Arbor, Michigan 48109, USA*

²*Theoretical Division, T-4, Los Alamos National Laboratory, Los Alamos, New Mexico 87545, USA*

³*Theoretical Division, T-4 and CNLS, Los Alamos National Laboratory, Los Alamos, New Mexico 87545, USA*
(Dated: December 7, 2021)

Moiré superlattice realized in two-dimensional heterostructures offers an exciting platform to access strongly-correlated electronic states. In this work, we study transition metal dichalcogenides (TMD) Moiré superlattices with time-reversal symmetry and nontrivial spin/valley-Chern numbers. Utilizing realistic material parameters and the method of exact diagonalization, we find that at certain twisting angle and fractional filling, gapped fractional topological states, i.e., fractional Chern insulators, are naturally stabilized by simply introducing the Coulomb repulsion. In contrast to fractional quantum Hall systems, where the time-reversal symmetry has to be broken explicitly, these fractional states break the time-reversal symmetry spontaneously. We show that the Chern number contrasting in the opposite valleys imposes a strong constraint on the nature of fractional Chern insulator and the associated low energy excitations.

Introduction.— When two layers of two-dimensional materials are placed atop of each other with slight misalignment, it creates a superlattice with periodicity much larger than the atomic lattice parameter. Because of the large lattice periodicity, one can fill or empty the entire band by electrode gating. This Moiré superlattice provides a tunable platform to control the electronic band structure [1, 2], and therefore enables access to a plethora of interesting quantum states. Because the band width in these systems can be tuned to be extremely narrow [2], these Moiré superlattices open up a new pathway to stabilize various strongly-correlated phases such as superconductivity and correlated insulators [3–27]. Furthermore, such electronic band structure can also be topologically nontrivial, e.g., with a nonzero integer Chern number [28–32]. Combined with their strong coupling nature, such Moiré superlattices offer a promising route to realize the long-sought fractionalized topological order [33–39].

Recently, gapped electronic states at various fractional fillings (e.g., $1/3$) were observed in transition metal dichalcogenide (TMD) Moiré superlattices, e.g., WSe_2/WS_2 [18, 40–43]. In general, gapped electronic states at fractional filling may have two origins: (a) charge order that spontaneously breaks the translational symmetry and (b) fractional topological order, e.g., fractional Chern insulators (FCI) [44–51]. In these TMD Moiré superlattices, the observed gapped states were interpreted as Wigner crystals of electrons, because the underlying single-particle bands are topologically trivial [52].

Encouraged by such exciting experimental progress, here we explore the feasibility of the second category in TMD Moiré superlattices. In particular, we focus on systems like MoTe_2 , which may host topologically nontrivial bands with non-zero spin/valley-Chern numbers [53]. In contrast to a partially filled Chern band [44–51], because these systems preserve the time-reversal symmetry, two types of fractional states are in principle allowed (a) time-reversal invariant fractional topological insulators [54] and (b) FCIs via spontaneously breaking the time-reversal symmetry. The key focus of this study is whether Coulomb repulsion could stabilize some of these fractional states in TMD Moiré superlattices.

In this work, we show that by simply increasing the Coulomb interaction strength in such TMD Moiré superlattices, the system undergoes a quantum phase transition that spontaneously breaks the time-reversal symmetry by polarizing electrons into one of the two valleys. Further increase of Coulomb interaction will trigger a second quantum phase transition, and stabilize a FCI at a fractional filling. For excitations, our numerical studies observe both (intravalley) fractional excitations from the fractional topological order and (intervalley) valley-wave excitations from the spontaneous symmetry breaking. We argue that the symmetry breaking state and low-energy excitations are constrained by the valley contrasting Chern number in TMD Moiré superlattice.

Model.— We consider twisted homobilayer TMD materials. For each single layer, the low energy electronic states reside at the valence band maxima at $\pm\mathbf{K}$ valleys. Contrary to bilayer graphene systems where the valley and spin degrees of freedom are both present, in TMD each valley in the top valence band has fixed spin orientation due to strong spin-orbit coupling and the broken inversion symmetry [55]. With a small twist angle θ between two layers, the $+\mathbf{K}$ valley for the top and bottom layers are shifted to \mathbf{K}_t and \mathbf{K}_b in the Moiré Brillouin zone (MBZ) respectively, [Fig. 1(b)]. For convenience we choose the rhombus-shaped MBZ and set the point $\mathbf{M} = (\mathbf{K}_t + \mathbf{K}_b)/2$ as the origin. We employ the continuum model [2] in which the Moiré Hamiltonian for the $+\mathbf{K}$ valley is:

$$H_+(\mathbf{k}, \mathbf{r}) = \begin{pmatrix} -\frac{\hbar^2(\mathbf{k}-\mathbf{K}_b)^2}{2m^*} + \Delta_b(\mathbf{r}) & \Delta_T(\mathbf{r}) \\ \Delta_T^\dagger(\mathbf{r}) & -\frac{\hbar^2(\mathbf{k}-\mathbf{K}_t)^2}{2m^*} + \Delta_t(\mathbf{r}) \end{pmatrix} \quad (1)$$

Here m^* is the effective mass. The form of Moiré potential, $\Delta_{b,t,T}$, is dictated by the D_3 crystalline symmetry and a combination of C_{2z} rotation followed by switching the two layers, and can be parameterized by [53]:

$$\begin{aligned} \Delta_T(\mathbf{r}) &= w \left(1 + e^{-i\mathbf{G}_2 \cdot \mathbf{r}} + e^{-i\mathbf{G}_3 \cdot \mathbf{r}} \right) \\ \Delta_I(\mathbf{r}) &= 2w_z \sum_{j=1,3,5} \cos(\mathbf{G}_j \cdot \mathbf{r} + l\psi), \end{aligned} \quad (2)$$

where $l \in \{b, t\} = \{+1, -1\}$ and \mathbf{G}_j is the Moiré reciprocal lattice vectors with length $|\mathbf{G}_j| = \frac{4\pi}{\sqrt{3}a_M}$ and polar angle $\frac{\pi(j-1)}{3}$. Here $a_M = a_0/\theta$ is the Moiré lattice constant for a small twisted angle θ and a_0 is the lattice parameter of TMD. The Hamiltonian for the valley $-\mathbf{K}$ can be obtained by the time-reversal symmetry $H_-(\mathbf{k}, \mathbf{r}) = H_+(-\mathbf{k}, \mathbf{r})^*$. To be specific, we focus on twisted MoTe₂ homobilayer with typical parameters ($\hbar^2/2m^*a_0^2$, w_z , w , ψ) = (495 meV, 8 meV, -8.5 meV, -89.6°) [53].

The top valence band of a TMD single layer splits into multiple Moiré bands due to the Moiré potential. As shown in Fig. 1(c) and (d), when the twist angle is close to $\theta_0 = 1.38^\circ$, the top Moiré band becomes nearly flat. The flatness of a band can be characterized by a ratio of the gap between the nearest bands to its band width. For the top Moiré band, the ratio can be as large as 13. When $\theta < 3.1^\circ$, The top Moiré band is topological characterized by a valley/spin Chern number $C = \pm 1$ due to the skyrmion lattice pseudo spin textures of the Moiré potential [53]. The Chern number for the opposite valley/spin is opposite as required by time-reversal symmetry. Thus, at the single-particle level, such TMD homobilayer realizes a quantum valley/spin Hall insulator.

We then introduce screened Coulomb interaction and project it to the nearly flat top Moiré band [56]:

$$\begin{aligned} H_{\text{int}} &= \frac{1}{2A} \sum_{\mathbf{q}} : \rho(\mathbf{q})V(\mathbf{q})\rho(-\mathbf{q}) : \\ &= \sum_{\mathbf{k}, \mathbf{k}', \mathbf{q}, \tau, \tau'} \frac{U}{2N_{\text{cell}}} v(\mathbf{q}) \lambda_{\tau, \mathbf{q}}(\mathbf{k}) \lambda_{\tau', \mathbf{q}}(\mathbf{k}')^* \\ &\quad C_{\tau}^{\dagger}(\mathbf{k}) C_{\tau'}^{\dagger}(\mathbf{k}' + \mathbf{q}) C_{\tau'}(\mathbf{k}') C_{\tau}(\mathbf{k} + \mathbf{q}), \end{aligned} \quad (3)$$

where $\tau = \pm$ is the valley index, and $\lambda_{\tau, \mathbf{q}}(\mathbf{k}) = \langle u_{\tau, \mathbf{k}} | u_{\tau, \mathbf{k} + \mathbf{q}} \rangle$ is the form factor originated from the projection. Here $v(\mathbf{q}) = 4\pi \tanh(qd)/\sqrt{3}qa_M$ is the dimensionless screened Coulomb potential with d the separation between the electrode and Moiré superlattice, which is set to $d = 2a_M$ in the calculations. A is system area and N_{cell} is the number of the unit cells in the calculations. The coefficient of $v(\mathbf{q})$ is chosen to make U equal to the bare Coulomb potential between two particles separated by a_M . $C_{\tau}(\mathbf{k})$ is the annihilation operator for single particle state $|u_{\tau, \mathbf{k}}\rangle$. We neglect the weak intervalley impurity scattering process associated with a large momentum transfer, and therefore the Hamiltonian also has a valley $U(1)_v$ symmetry. In this model, there are two competing symmetry breaking states: an intervalley coherent state that breaks the valley $U(1)_v$ symmetry and an valley/spin polarized state that breaks the time reversal symmetry. At half filling of the topmost band (account for valley degree of freedom), our Hartree-Fock analysis and exact-diagonalization results both suggest that a valley-polarized state is energetically favored, which spontaneously breaks the time-reversal symmetry and leads to a interaction-induced Chern insulator [57]. At fractional filling, in principle, two types of fractional topological states might emerge, a fractional Chern insulator or a fractional topological insulator [54, 58], depending on whether

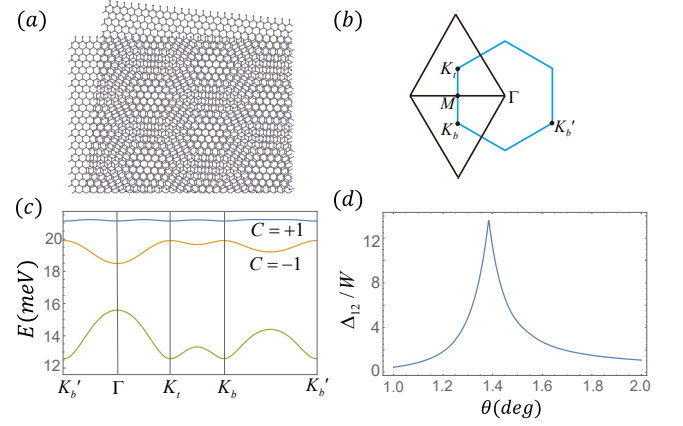


FIG. 1. (a): Schematic view of the Moiré superlattice. (b): We choose the Moiré Brillouin zone (MBZ) to be the rhombus and the origin in momentum space is chosen at M . (c): Moiré band structure at $\theta = 1.38^\circ$. The top Moiré band is nearly flat with Chern number ± 1 . (d): The gap ratio $\frac{\Delta_{12}}{W} = \frac{\min(E_1(\mathbf{k})) - \max(E_2(\mathbf{k}))}{\max(E_1(\mathbf{k})) - \min(E_1(\mathbf{k}))}$ as a function of twisted angle θ , where $E_1(\mathbf{k})$ ($E_2(\mathbf{k})$) is the energy of the first (second) topmost Moiré band.

the time-reversal symmetry is spontaneously broken or preserved [59], and our exact diagonalization below show that the FCI is favored and stabilized in our system.

Valley polarized FCI.— We define the filling factor $\nu = 2\rho_e/\rho_s$, where ρ_e is the electron density occupying the top Moiré band and ρ_s is the electron density for the full filling of the two-fold degenerate top Moiré band. The factor 2 accounts for the valley degree of freedom. Using exact diagonalization, at $\nu = 1/3$ we observe numerical evidence of spontaneous valley polarization and FCI in the strong interaction limit, as shown in Fig. 2(a). For 8 electrons in 4×6 unit cells ($4 \times 6 \times 2$ single-particle states including both valleys), the ground states are fully valley polarized with three nearly-degenerate ground states for each valley polarization, separated from the excited states by an energy gap of the order of 2 K. We calculated the many-body Chern number of each ground state [48], and the topological index is found to be $1/3$, characterizing a $1/3$ FCI phase. This conclusion is further supported by the total momentum for each ground state, which obeys the generalized Pauli exclusion rule [60].

The occupation number $n(k_1, k_2)$ of single particle states for each of the three many-body ground states are plotted in Fig. 2(b). $n(k_1, k_2)$ is uniformly distributed for different single particle states, consistent with the fact that the ground state is an incompressible liquid. The spectrum evolution under flux insertion along k_2 direction is shown in Fig. 2(c). The excitation gap is maintained throughout the flux insertion process.

The topological nature of the ground states are further confirmed by our calculation of the particle entanglement spectrum (PES) [60]. To compute PES, we divide the N particles into two collections of N_A and $N_B = N - N_A$ particles and trace out N_B particles to get the reduced density matrix ρ_A .

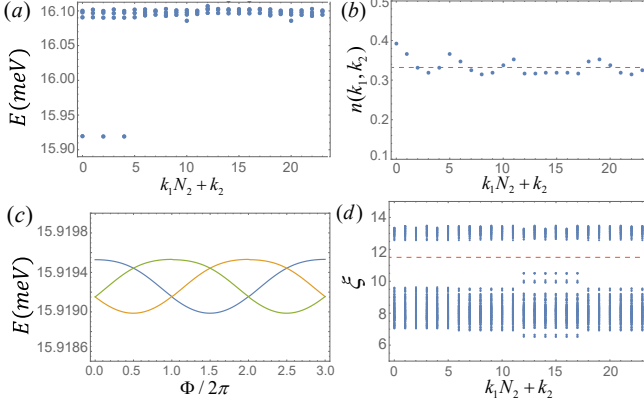


FIG. 2. Numerical diagonalization results for 8 particles in 4×6 Moiré lattice. We choose $\theta = 1.38^\circ$ and $U = 1.38$ meV. The bandwidth at this twist angle is $W = 0.083$ meV. Here $N = N_1 \times N_2/3$ is the number of particles. (a): Energy spectrum with three nearly degenerate ground states in each valley. (b): The occupation number of single particle states $n(k_1, k_2)$ for each of the three many-body ground states. The nearly uniform distribution of $n(k_1, k_2)$ suggests the ground state is an incompressible liquid. (c): Under flux insertion along k_2 direction, the ground states evolve into each other. (d): Particle entanglement spectrum (PES) for the separation of $N_A = 4$ particles.

The PES levels ξ are obtained from the logarithm of eigenvalues of ρ_A , and are labeled by the total momentum of the remaining N_A particles, as shown in Fig. 2(d). There is a clear entanglement gap with 2730 levels below the gap for $N_A = 4$, consistent with the counting of quasi-hole excitation in the $\nu = 1/3$ FCI [60].

To exam the finite-size effect, we study the scaling of the many-body gap Δ with various system sizes. For a genuine FCI, Δ remain finite in the thermodynamic limit when both N_1 and N_2 approach infinity. However Δ should vanish if only one of N_1 or N_2 approaches infinity, because this limit is a one-dimensional system which should not support FCI [47]. This is confirmed in Fig. 3(a), which shows Δ decreases when N_1 is fixed at 3 and N_2 increases from 4 to 8, but Δ increases when the system size changes from 3×8 to 4×6 .

We then map out the phase diagram at $\nu = 1/3$ filling as a function of the interaction strength U which can be controlled by distance between the electrodes and the Moiré superlattice in experiments and the dielectric constant ϵ . The results are shown in Fig. 3(b). We find a valley non-polarized Fermi liquid at a small $1/\epsilon$ corresponding to a small U , a Fermi liquid with valley polarization at an intermediate interaction and the FCI phase with valley polarization at strong interaction. Depending on the twisted angle θ , which controls the bandwidth, the valley non-polarized Fermi liquid can transit directly to FCI with valley polarization or through an intermediate Fermi liquid with valley polarization. The phase transition between the valley-polarized Fermi liquid and FCI can be described by Ginzburg-Landau theory with a Chern-Simons term [57]. The direct transition occurs near $\theta = 1.38^\circ$ where the single parti-

cle Moiré band has the largest gap to bandwidth ratio [see Fig. 1(d)]. This is consistent with the quantum Hall systems with flat Landau levels, where the interaction stabilizes simultaneously the fractional quantum Hall state with spin polarization. Note that the FCI can be stabilized in a relatively broader region of the twisted angle here compared to that in magic angle twisted bilayer graphene [33–39], and the region of angle for FCI increases with interaction. For interaction above the dashed line in Fig. 3(b), our single-band approximation used in the numerical calculations breaks down and it requires to take other nearby bands into account.

Excitations.— Here we study the charge neutral excitations above the FCI ground states. As a consequence of the spontaneous valley polarization, we consider the valley waves excitation $|\Psi_v(\mathbf{q})\rangle = \sum_{\mathbf{k}} z_{\mathbf{k}} C_+^\dagger(\mathbf{k} + \mathbf{q}) C_- (\mathbf{k}) |\Psi_-\rangle$, where $|\Psi_-\rangle$ is the FCI ground state with $\tau = -$ valley fully occupied and $z_{\mathbf{k}}$ is variational parameter. The presence of the form factor in Eq. (3) breaks the valley pseudospin $SU(2)$ rotation system down to the valley $U(1)_v$ symmetry. As a result, the valley wave excitation are gapped as shown in Fig. 4, which can be fitted by $E_w(\mathbf{q}) = Jq^2 + A$. The valley wave disperses weakly in momentum and thus is well localized in real space.

The lowest intravalley many-body excitation has lower energy than valley wave excitation for the parameters we used, i.e., the energy difference between the lowest fully-polarized excited state and the FCI state is $E_{mb} = 0.167$ meV $< E_w$, see Fig. 4. Nevertheless, the valley wave excitation remains a stable excitation because the decay of the valley wave to the intravalley many-body excitations are forbidden. Intravalley many-body excitations has valley quantum number 0, while the valley wave has valley quantum number 2.

In quantum Hall ferromagnets, a pair of skyrmions has lower energy than the particle-hole bound state [61]. The system size limitation in the exact diagonalization does not allow us to study the valley skyrmion excitation in our numerical calculations. Here we use an effective Hamiltonian density for

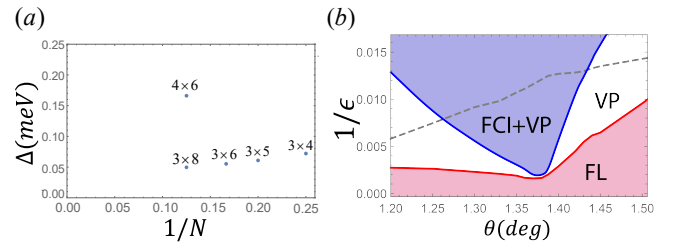


FIG. 3. (a): The many-body gap Δ for various system sizes at $\nu = 1/3$ filling. The interaction strength is fixed to be $U = 1.38$ meV. The increase of Δ in 4×6 system suggests the gap persists in the two-dimensional thermodynamic limit. (b): The phase diagram for Fermi liquid (FL), FL with valley polarization (VP) and fractional Chern insulator (FCI) at different interaction strength $U(\epsilon) = \frac{e^2}{4\pi\epsilon\epsilon_0 a_M}$ and twisted angle θ . The dashed line corresponds to $U(\epsilon) = \Delta_{12}$, above which the interaction starts to mix different bands and the single-band approximation breaks down.

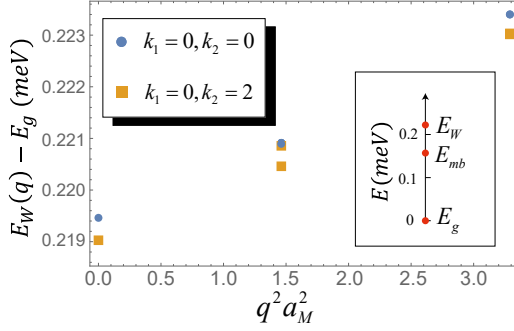


FIG. 4. Dispersion of valley wave excitation $E_w(\mathbf{q})$ for 8 particles in 4×6 lattice. Excitation above the ground state with total momentum $k_1 = 0, k_2 = 0$ ($k_1 = 0, k_2 = 2$) are labeled by the squares and circles respectively. The slight energy difference for these two ground states is caused by finite size effect. The inset compares the energy of the lowest valley wave excitation E_w , the lowest intravalley many-body excitation E_{mb} and the ground state energy E_g .

valley pseudospin $\mathbf{n}(\mathbf{r})$ [61]

$$H_n(\mathbf{r}) = \frac{J}{2}(\nabla \mathbf{n})^2 - \frac{A}{2}n_z^2 + \frac{1}{2} \int d\mathbf{r}' V(\mathbf{r} - \mathbf{r}') \rho_s(\mathbf{r}) \rho_s(\mathbf{r}'), \quad (4)$$

where J and A are given by the valley wave spectrum. The presence of the valley pseudospin anisotropy can be traced back to the opposite Chern number for the opposite valley. One cannot rotate \mathbf{n} from one valley to opposite valley adiabatically without closing the energy gap, which implies the existence of anisotropy for \mathbf{n} . The last term accounts for the Coulomb interaction $V(\mathbf{r} - \mathbf{r}')$, because a skyrmion is dressed with charge distribution $\rho_s(\mathbf{r}) = \epsilon^{ij} \epsilon_{abc} n^a \partial_i n^b \partial_j n^c / 8\pi$, where ϵ_{abc} (ϵ^{ij}) is the Levi-Civita tensor with i, j being the space index and a, b, c being the spin index. The skyrmion topological charge $Q_s = \int d\mathbf{r}^2 \rho_s(\mathbf{r})$ is quantized to an integer number. The easy axis anisotropy favors skyrmions with a small radius while the Coulomb repulsion favors skyrmions with a large radius. Their competition determines the skyrmion size [62].

FCI at $\nu = 2/5$.— In twisted graphene Moiré superlattices, the Halperin (332) state is stabilized at $\nu = 2/5$ due to the remaining SU(2) spin rotation symmetry in the valley polarized state [36]. In our TMD Moiré superlattices, the spin rotation symmetry is absent because of the spin-valley locking. The Chern number contrasting valley degree of freedom disfavors the (332) state. To demonstrate this explicitly, we calculate the energy spectrum, spectrum flow under flux insertion and entanglement spectrum at $\nu = 2/5$, and the results are displayed in Fig. 5. The 5-fold degenerate ground states are valley polarized, and are consistent with the $\nu = 2/5$ FCI state. In the fractional quantum Hall, the $\nu = 2/5$ state belongs to the second hierarchical Jain state, and similarly one can assign the $\nu = 2/5$ FCI as a second hierarchical FCI. Our results highlight the importance of symmetry in dictating the ground state and contrast the difference between the graphene and TMD Moiré superlattices.

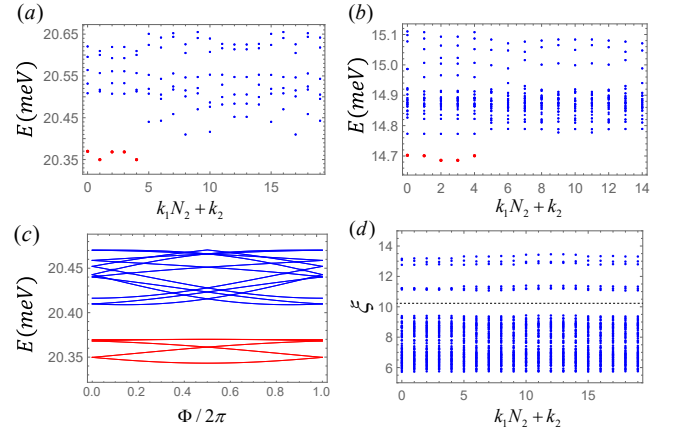


FIG. 5. FCI at $\nu = 2/5$. (a): the energy spectrum of 8 particles in 4×5 system, and (b): 6 particles in 3×5 system. (c): the flux insertion for the system in (a), where the five ground states are marked in red (some of them are on top of each other). A finite gap remains during flux insertion. (d): the particle entanglement spectrum for (a) with $N_A = 3$. There are $51 \times 20 = 1020$ states below the dashed line, consistent with quasihole counting.

Discussions.— We show that TMD Moiré superlattices can host fractional topological states via spontaneously breaking the time-reversal symmetry, using realistic parameters of TMD Moiré superlattices. Comparing with graphene, the spin-valley locking in TMD materials breaks the SU(2) spin rotation symmetry and eliminates the spin wave Goldstone modes, which could help stabilize the FCI states. The valley contrasting Chern number in TMD Moiré superlattices also dictates the symmetry breaking states, hence the nature of fractionalized topological states, and also the low energy excitations in the FCI. The gapped nature of these states can be detected by transport, optical measurements etc, and its topological nature can be accessed by Hall conductivity measurement. Due to the strong analogy between FCI and chiral spin liquids, it is plausible that Moiré superlattices may also help realize/stabilize exotic spin liquid phases [63–65] by unitizing the valley/layer pseudospin or real spin degrees of freedom.

Acknowledgements.— This work done at LANL was carried out under the auspices of the U.S. DOE NNSA under contract No. 89233218CNA000001 through the LDRD Program. S. Z. L. was also supported by the U.S. Department of Energy, Office of Science, Basic Energy Sciences, Materials Sciences and Engineering Division, Condensed Matter Theory Program. H.L. and K.S. acknowledge support through NSF Grant No. NSF-EFMA-1741618.

-
- [1] J. M. B. Lopes dos Santos, N. M. R. Peres, and A. H. Castro Neto, “Graphene bilayer with a twist: Electronic structure,” *Phys. Rev. Lett.* **99**, 256802 (2007).
 - [2] Rafi Bistritzer and Allan H. MacDonald, “Moiré bands in twisted double-layer graphene,” *PNAS* **108**, 12233–12237

- (2011).
- [3] Yuan Cao, Valla Fatemi, Ahmet Demir, Shiang Fang, Spencer L. Tomarken, Jason Y. Luo, Javier D. Sanchez-Yamagishi, Kenji Watanabe, Takashi Taniguchi, Efthimios Kaxiras, Ray C. Ashoori, and Pablo Jarillo-Herrero, “Correlated insulator behaviour at half-filling in magic-angle graphene superlattices,” *Nature* **556**, 80–84 (2018).
 - [4] Yuan Cao, Valla Fatemi, Shiang Fang, Kenji Watanabe, Takashi Taniguchi, Efthimios Kaxiras, and Pablo Jarillo-Herrero, “Unconventional superconductivity in magic-angle graphene superlattices,” *Nature* **556**, 43–50 (2018).
 - [5] Xiaobo Lu, Petr Stepanov, Wei Yang, Ming Xie, Mohammed Ali Aamir, Ipsita Das, Carles Urgell, Kenji Watanabe, Takashi Taniguchi, Guangyu Zhang, Adrian Bachtold, Allan H. MacDonald, and Dmitri K. Efetov, “Superconductors, orbital magnets and correlated states in magic-angle bilayer graphene,” *Nature* **574**, 653–657 (2019).
 - [6] Matthew Yankowitz, Shaowen Chen, Hryhorii Polshyn, Yuxuan Zhang, K. Watanabe, T. Taniguchi, David Graf, Andrea F. Young, and Cory R. Dean, “Tuning superconductivity in twisted bilayer graphene,” *Science* **363**, 1059–1064 (2019).
 - [7] Alexander Kerelsky, Leo J McGilly, Dante M Kennes, Lede Xian, Matthew Yankowitz, Shaowen Chen, K Watanabe, T Taniguchi, James Hone, Cory Dean, *et al.*, “Maximized electron interactions at the magic angle in twisted bilayer graphene,” *Nature* **572**, 95–100 (2019).
 - [8] Yuan Cao, Debanjan Chowdhury, Daniel Rodan-Legrain, Oriol Rubies-Bigordà, Kenji Watanabe, Takashi Taniguchi, T Senthil, and Pablo Jarillo-Herrero, “Strange metal in magic-angle graphene with near planckian dissipation,” *arXiv preprint arXiv:1901.03710* (2019).
 - [9] Hryhorii Polshyn, Matthew Yankowitz, Shaowen Chen, Yuxuan Zhang, K Watanabe, T Taniguchi, Cory R Dean, and Andrea F Young, “Large linear-in-temperature resistivity in twisted bilayer graphene,” *Nature Physics* **15**, 1011–1016 (2019).
 - [10] Yonglong Xie, Biao Lian, Berthold Jäck, Xiaomeng Liu, Cheng-Li Chiu, Kenji Watanabe, Takashi Taniguchi, B Andrei Bernevig, and Ali Yazdani, “Spectroscopic signatures of many-body correlations in magic-angle twisted bilayer graphene,” *Nature* **572**, 101–105 (2019).
 - [11] Yuhang Jiang, Xinyuan Lai, Kenji Watanabe, Takashi Taniguchi, Kristjan Haule, Jinhai Mao, and Eva Y Andrei, “Charge order and broken rotational symmetry in magic-angle twisted bilayer graphene,” *Nature* **573**, 91–95 (2019).
 - [12] Youngjoon Choi, Jeannette Kemmer, Yang Peng, Alex Thomson, Harpreet Arora, Robert Polski, Yiran Zhang, Hechen Ren, Jason Alicea, Gil Refael, *et al.*, “Electronic correlations in twisted bilayer graphene near the magic angle,” *Nature Physics* **15**, 1174–1180 (2019).
 - [13] U. Zondiner, A. Rozen, D. Rodan-Legrain, Y. Cao, R. Queiroz, T. Taniguchi, K. Watanabe, Y. Oreg, F. von Oppen, Ady Stern, E. Berg, P. Jarillo-Herrero, and S. Ilani, “Cascade of phase transitions and Dirac revivals in magic-angle graphene,” *Nature* **582**, 203–208 (2020), number: 7811 Publisher: Nature Publishing Group.
 - [14] Dillon Wong, Kevin P. Nuckolls, Myungchul Oh, Biao Lian, Yonglong Xie, Sangjun Jeon, Kenji Watanabe, Takashi Taniguchi, B. Andrei Bernevig, and Ali Yazdani, “Cascade of electronic transitions in magic-angle twisted bilayer graphene,” *Nature* **582**, 198–202 (2020), number: 7811 Publisher: Nature Publishing Group.
 - [15] Kevin P. Nuckolls, Myungchul Oh, Dillon Wong, Biao Lian, Kenji Watanabe, Takashi Taniguchi, B. Andrei Bernevig, and Ali Yazdani, “Strongly correlated Chern insulators in magic-angle twisted bilayer graphene,” *Nature* **588**, 610–615 (2020), number: 7839 Publisher: Nature Publishing Group.
 - [16] Minhao He, Yuhao Li, Jiaqi Cai, Yang Liu, K. Watanabe, T. Taniguchi, Xiaodong Xu, and Matthew Yankowitz, “Symmetry breaking in twisted double bilayer graphene,” *Nature Physics* , 1–5 (2020), publisher: Nature Publishing Group.
 - [17] Xiaomeng Liu, Zeyu Hao, Eslam Khalaf, Jong Yeon Lee, Yuval Ronen, Hyobin Yoo, Danial Haei Najafabadi, Kenji Watanabe, Takashi Taniguchi, Ashvin Vishwanath, and Philip Kim, “Tunable spin-polarized correlated states in twisted double bilayer graphene,” *Nature* **583**, 221–225 (2020), number: 7815 Publisher: Nature Publishing Group.
 - [18] Emma C. Regan, Danqing Wang, Chenhao Jin, M. Iqbal Bakti Utama, Beini Gao, Xin Wei, Sihan Zhao, Wenyu Zhao, Zuocheng Zhang, Kentaro Yumigeta, Mark Blei, Johan D. Carlström, Kenji Watanabe, Takashi Taniguchi, Sefaattin Tongay, Michael Crommie, Alex Zettl, and Feng Wang, “Mott and generalized Wigner crystal states in WSe₂/WS₂ moiré superlattices,” *Nature* **579**, 359–363 (2020), number: 7799 Publisher: Nature Publishing Group.
 - [19] Lei Wang, En-Min Shih, Augusto Ghiotto, Lede Xian, Daniel A. Rhodes, Cheng Tan, Martin Claassen, Dante M. Kennes, Yuesong Bai, Bumho Kim, Kenji Watanabe, Takashi Taniguchi, Xiaoyang Zhu, James Hone, Angel Rubio, Abhay N. Pasupathy, and Cory R. Dean, “Correlated electronic phases in twisted bilayer transition metal dichalcogenides,” *Nature Materials* **19**, 861–866 (2020), number: 8 Publisher: Nature Publishing Group.
 - [20] Ming Xie and A. H. MacDonald, “Nature of the correlated insulator states in twisted bilayer graphene,” *Phys. Rev. Lett.* **124**, 097601 (2020).
 - [21] Fengcheng Wu and Sankar Das Sarma, “Collective excitations of quantum anomalous hall ferromagnets in twisted bilayer graphene,” *Phys. Rev. Lett.* **124**, 046403 (2020).
 - [22] Ying Su and Shi-Zeng Lin, “Current-induced reversal of anomalous hall conductance in twisted bilayer graphene,” *Phys. Rev. Lett.* **125**, 226401 (2020).
 - [23] Bikash Padhi, Chandan Setty, and Philip W. Phillips, “Doped twisted bilayer graphene near magic angles: Proximity to wigner crystallization, not mott insulation,” *Nano Letters* **18**, 6175–6180 (2018), PMID: 30185049, <https://doi.org/10.1021/acs.nanolett.8b02033>.
 - [24] Bikash Padhi, R. Chitra, and Philip W. Phillips, “Generalized wigner crystallization in moiré materials,” (2020), *arXiv:2009.13536 [cond-mat.str-el]*.
 - [25] Bikash Padhi and Philip W. Phillips, “Pressure-induced metal-insulator transition in twisted bilayer graphene,” *Phys. Rev. B* **99**, 205141 (2019).
 - [26] Nikolaos Stefanidis and Inti Sodemann, “Excitonic Laughlin states in ideal topological insulator flat bands and their possible presence in moiré superlattice materials,” *Phys. Rev. B* **102**, 035158 (2020).
 - [27] Nick Bultinck, Shubhayu Chatterjee, and Michael P. Zaletel, “Mechanism for anomalous hall ferromagnetism in twisted bilayer graphene,” *Phys. Rev. Lett.* **124**, 166601 (2020).
 - [28] Ya-Hui Zhang, Dan Mao, Yuan Cao, Pablo Jarillo-Herrero, and T. Senthil, “Nearly flat chern bands in moiré superlattices,” *Phys. Rev. B* **99**, 075127 (2019).
 - [29] Cécile Repellin, Zhihuan Dong, Ya-Hui Zhang, and T. Senthil, “Ferromagnetism in narrow bands of moiré superlattices,” *Phys. Rev. Lett.* **124**, 187601 (2020).
 - [30] Aaron L. Sharpe, Eli J. Fox, Arthur W. Barnard, Joe Finney, Kenji Watanabe, Takashi Taniguchi, M. A. Kastner, and David Goldhaber-Gordon, “Emergent ferromagnetism near

- three-quarters filling in twisted bilayer graphene,” *Science* **365**, 605–608 (2019).
- [31] M. Serlin, C. L. Tschirhart, H. Polshyn, Y. Zhang, J. Zhu, K. Watanabe, T. Taniguchi, L. Balents, and A. F. Young, “Intrinsic quantized anomalous hall effect in a moiré heterostructure,” *Science* (2019), 10.1126/science.aay5533.
- [32] Guorui Chen, Aaron L Sharpe, Eli J Fox, Ya-Hui Zhang, Shaoxin Wang, Lili Jiang, Bosai Lyu, Hongyuan Li, Kenji Watanabe, Takashi Taniguchi, *et al.*, “Tunable correlated chern insulator and ferromagnetism in trilayer graphene/boron nitride moiré superlattice,” arXiv preprint arXiv:1905.06535 (2019).
- [33] Patrick J. Ledwith, Grigory Tarnopolsky, Eslam Khalaf, and Ashvin Vishwanath, “Fractional chern insulator states in twisted bilayer graphene: An analytical approach,” *Phys. Rev. Research* **2**, 023237 (2020).
- [34] Cécile Repellin and T. Senthil, “Chern bands of twisted bilayer graphene: Fractional chern insulators and spin phase transition,” *Phys. Rev. Research* **2**, 023238 (2020).
- [35] Ahmed Abouelkomsan, Zhao Liu, and Emil J. Bergholtz, “Particle-hole duality, emergent fermi liquids, and fractional chern insulators in moiré flatbands,” *Phys. Rev. Lett.* **124**, 106803 (2020).
- [36] Zhao Liu, Ahmed Abouelkomsan, and Emil J. Bergholtz, “Gate-tunable fractional chern insulators in twisted double bilayer graphene,” *Phys. Rev. Lett.* **126**, 026801 (2021).
- [37] Patrick Wilhelm, Thomas C. Lang, and Andreas M. Läuchli, “Interplay of Fractional Chern Insulator and Charge-Density-Wave Phases in Twisted Bilayer Graphene,” arXiv:2012.09829 [cond-mat] (2020), arXiv: 2012.09829.
- [38] Ramanjit Sohal, Luiz H. Santos, and Eduardo Fradkin, “Chern-simons composite fermion theory of fractional chern insulators,” *Phys. Rev. B* **97**, 125131 (2018).
- [39] Ramanjit Sohal and Eduardo Fradkin, “Intertwined order in fractional chern insulators from finite-momentum pairing of composite fermions,” *Phys. Rev. B* **101**, 245154 (2020).
- [40] Yang Xu, Song Liu, Daniel A. Rhodes, Kenji Watanabe, Takashi Taniguchi, James Hone, Veit Elser, Kin Fai Mak, and Jie Shan, “Correlated insulating states at fractional fillings of moiré superlattices,” *Nature* **587**, 214–218 (2020), number: 7833 Publisher: Nature Publishing Group.
- [41] Chenhao Jin, Zui Tao, Tingxin Li, Yang Xu, Yanhao Tang, Jiacheng Zhu, Song Liu, Kenji Watanabe, Takashi Taniguchi, James C. Hone, Liang Fu, Jie Shan, and Kin Fai Mak, “Stripe phases in WSe₂/WS₂ moiré superlattices,” arXiv:2007.12068 [cond-mat] (2020), arXiv: 2007.12068.
- [42] You Zhou, Jiho Sung, Elise Brutschea, Ilya Esterlis, Yao Wang, Giovanni Scuri, Ryan J. Gelly, Hoseok Heo, Takashi Taniguchi, Kenji Watanabe, Gergely Zaránd, Mikhail D. Lukin, Philip Kim, Eugene Demler, and Hongkun Park, “Signatures of bilayer Wigner crystals in a transition metal dichalcogenide heterostructure,” arXiv:2010.03037 [cond-mat] (2020), arXiv: 2010.03037.
- [43] Xiong Huang, Tianmeng Wang, Shengnan Miao, Chong Wang, Zhipeng Li, Zhen Lian, Takashi Taniguchi, Kenji Watanabe, Satoshi Okamoto, Di Xiao, Su-Fei Shi, and Yong-Tao Cui, “Correlated Insulating States at Fractional Fillings of the WS₂/WSe₂ Moiré Lattice,” arXiv:2007.11155 [cond-mat] (2020), arXiv: 2007.11155.
- [44] Evelyn Tang, Jia-Wei Mei, and Xiao-Gang Wen, “High-temperature fractional quantum hall states,” *Phys. Rev. Lett.* **106**, 236802 (2011).
- [45] Kai Sun, Zhengcheng Gu, Hosho Katsura, and S. Das Sarma, “Nearly flatbands with nontrivial topology,” *Phys. Rev. Lett.* **106**, 236803 (2011).
- [46] Titus Neupert, Luiz Santos, Claudio Chamon, and Christopher Mudry, “Fractional quantum hall states at zero magnetic field,” *Phys. Rev. Lett.* **106**, 236804 (2011).
- [47] N. Regnault and B. Andrei Bernevig, “Fractional chern insulator,” *Phys. Rev. X* **1**, 021014 (2011).
- [48] D. N. Sheng, Zheng-Cheng Gu, Kai Sun, and L. Sheng, “Fractional quantum hall effect in the absence of landau levels,” *Nature Communications* **2**, 389 (2011).
- [49] Siddharth A. Parameswaran, Rahul Roy, and Shivaji L. Sondhi, “Fractional quantum Hall physics in topological flat bands,” *Comptes Rendus Physique Topological insulators / Isolants topologiques*, **14**, 816–839 (2013).
- [50] Emil J. Bergholtz and Zhao Liu, “Topological flat band models and fractional chern insulators,” *International Journal of Modern Physics B* **27**, 1330017 (2013), publisher: World Scientific Publishing Co.
- [51] Yang-Le Wu, B. Andrei Bernevig, and N. Regnault, “Zoology of fractional chern insulators,” *Phys. Rev. B* **85**, 075116 (2012).
- [52] Fengcheng Wu, Timothy Lovern, Emanuel Tutuc, and A. H. MacDonald, “Hubbard model physics in transition metal dichalcogenide moiré bands,” *Phys. Rev. Lett.* **121**, 026402 (2018).
- [53] Fengcheng Wu, Timothy Lovern, Emanuel Tutuc, Ivar Martin, and A. H. MacDonald, “Topological insulators in twisted transition metal dichalcogenide homobilayers,” *Phys. Rev. Lett.* **122**, 086402 (2019).
- [54] Michael Levin and Ady Stern, “Fractional topological insulators,” *Phys. Rev. Lett.* **103**, 196803 (2009).
- [55] Di Xiao, Gui-Bin Liu, Wanxiang Feng, Xiaodong Xu, and Wang Yao, “Coupled spin and valley physics in monolayers of mos₂ and other group-vi dichalcogenides,” *Phys. Rev. Lett.* **108**, 196802 (2012).
- [56] Jong Yeon Lee, Eslam Khalaf, Shang Liu, Xiaomeng Liu, Zeyu Hao, Philip Kim, and Ashvin Vishwanath, “Theory of correlated insulating behaviour and spin-triplet superconductivity in twisted double bilayer graphene,” *Nature Communications* **10**, 5333 (2019).
- [57] See Supplemental Materials for (1) variational calculations of the energy for the valley polarized and intervalley coherent state, (2) Hartree-Fock calculations, (3) discussion on the possibility of the Halperin state and (4) effective theory for the transition between the valley polarized Fermi liquid and fractional Chern insulator.
- [58] Ady Stern, “Fractional Topological Insulators: A Pedagogical Review,” *Annual Review of Condensed Matter Physics* **7**, 349–368 (2016), publisher: Annual Reviews.
- [59] One may think of another possibility, analogous to the Halperin (m_1, m_2, n_1) states. However, this state is not favored because of the opposite Chern number in the opposite valley. [57].
- [60] B. Andrei Bernevig and N. Regnault, “Emergent many-body translational symmetries of abelian and non-abelian fractionally filled topological insulators,” *Phys. Rev. B* **85**, 075128 (2012).
- [61] S. L. Sondhi, A. Karlhede, S. A. Kivelson, and E. H. Rezayi, “Skyrmions and the crossover from the integer to fractional quantum hall effect at small zeeman energies,” *Phys. Rev. B* **47**, 16419–16426 (1993).
- [62] Shubhayu Chatterjee, Matteo Ippoliti, and Michael P. Zaletel, “Skyrmion Superconductivity: DMRG evidence for a topological route to superconductivity,” arXiv:2010.01144 [cond-mat] (2020), arXiv: 2010.01144.
- [63] Krishna Kumar, Kai Sun, and Eduardo Fradkin, “Chern-simons theory of magnetization plateaus of the spin- $\frac{1}{2}$ quantum xxz heisenberg model on the kagome lattice,” *Phys. Rev. B* **90**, 174409 (2014).

- [64] Krishna Kumar, Kai Sun, and Eduardo Fradkin, “Chiral spin liquids on the kagome lattice,” *Phys. Rev. B* **92**, 094433 (2015).
 - [65] W. Zhu, Shou-Shu Gong, Tian-Sheng Zeng, Liang Fu, and D. N. Sheng, “Interaction-driven spontaneous quantum hall effect on a kagome lattice,” *Phys. Rev. Lett.* **117**, 096402 (2016).
 - [66] Nick Bultinck, Eslam Khalaf, Shang Liu, Shubhayu Chatterjee, Ashvin Vishwanath, and Michael P. Zaletel, “Ground state and hidden symmetry of magic-angle graphene at even integer filling,” *Phys. Rev. X* **10**, 031034 (2020).
 - [67] Eduardo Fradkin, *Field Theories of Condensed Matter Physics*, 2nd ed. (Cambridge University Press, Cambridge, 2013).
 - [68] Hua Chen and Kun Yang, “Interaction-driven quantum phase transitions in fractional topological insulators,” *Phys. Rev. B* **85**, 195113 (2012).
-

Supplemental Material: Spontaneous fractional Chern insulators in transition-metal-dichalcogenides Moiré superlattices

I. Energy for valley polarized (VP) and intervalley coherent (IVC) state

Here we compare the energy for the valley polarized and intervalley coherent state. We consider half filling of the topmost band including the valley degree of freedom. The wave function for the VP state can be written as

$$|\Psi_{VP}\rangle = \prod_k C_+^\dagger(k) |0\rangle.$$

Here we choose $\tau = +$ valley to be fully occupied. Its energy $\langle \Psi_{VP} | H | \Psi_{VP} \rangle$ can be decomposed into single particle contribution $E_0 = \sum_k \epsilon_+(k)$; Hartree contribution: $E_{Ha} = V(0) [\sum_k \lambda_{+,0}(k)]^2$ and the Fock contribution: $E_{Fo} = - \sum_{k,q} V(q) |\lambda_{+,q}(k)|^2$. Here the summation of k is over the whole Moiré Brillouin zone.

We note that the system Hamiltonian is invariant under the following gauge transformation

$$C_\tau(k) \rightarrow \exp[i\theta_\tau(k)] C_\tau(k),$$

$$\lambda_{\tau,q}(k) \rightarrow \exp[i\theta_\tau(k) - \theta_\tau(k+q)] \lambda_{\tau,q}(k).$$

We choose a gauge which fixes the valley pseudospin associated with $|\Psi_{IVC}\rangle$ in the x direction, and the wave function of the intervalley coherent state can be written as

$$|\Psi_{IVC}\rangle = \frac{1}{\sqrt{2}} \prod_k [C_+^\dagger(k) + C_-^\dagger(k)] |0\rangle.$$

The energy for the IVC is the sum of single particle contribution $E'_0 = \sum_k [\epsilon_+(k) + \epsilon_-(k)]/2$; Hartree contribution: $E'_{Ha} = \frac{V(0)}{4} [\sum_{k,\tau=\pm} \lambda_{\tau,0}(k)]^2$ and the Fock contribution

$$E'_{Fo} = -\frac{1}{4} \sum_{k,q} V(q) [|\lambda_{+,q}(k)|^2 + |\lambda_{-,q}(k)|^2 + \lambda_{+,q}(k) \lambda_{-,q}(k+q) + \lambda_{-,q}(k) \lambda_{+,q}(k+q)].$$

It is easy to check that the single particle and Hartree part of the energy for the VP and IVC are the same. We compare the Fock part of the energy. Noticing that $\lambda_{\tau,-q}(k+q) = \lambda_{\tau,q}^*(k)$, we have

$$\lambda_{+,q}(k) \lambda_{-,q}(k+q) + \lambda_{-,q}(k) \lambda_{+,q}(k+q) \leq 2|\lambda_{+,q}(k) \lambda_{-,q}(k+q)|,$$

where the bound is saturated when $\lambda_{+,q}(k) \lambda_{-,q}(k+q)$ is positive real. The energy difference between the IVC and VP is

$$E'_{Fo} - E_{Fo} \geq \frac{1}{4} \sum_{k,q} V(q) [|\lambda_{+,q}(k)| - |\lambda_{-,q}(k)|]^2.$$

By considering time reversal operation and C_2 rotation combined with layer flipping symmetry, we can show $|\lambda_{+,q}(k)| = |\lambda_{-,q}(k)|$. After we choose the form of $|\Psi_{IVC}\rangle$ by fixing a gauge, it is not guaranteed that $\lambda_{+,q}(k) \lambda_{-,q}(k+q)$ is positive real for *all* k and q . Therefore the IVC always has higher energy than that of the VP state. This conclusion is further supported by more detailed Hartree-Fock calculations below.

II. Hartree-Fock calculations

We treat the interaction part of the Hamiltonian using Hartree-Fock mean-field theory [S66] in which the Hamiltonian can be written as

$$\mathcal{H}_{MF} = \sum_{k,\tau,\tau'} C_\tau^\dagger(\mathbf{k}) [(h_0(\mathbf{k}) - \mu) \delta_{\tau,\tau'} + h_{HF}^{\tau,\tau'}(\Delta_k, \mathbf{k})] C_{\tau'}(\mathbf{k}) - \frac{1}{2} \text{tr} h_{MF}(\Delta_k, \mathbf{k}) \Delta_k^T \quad (S1)$$

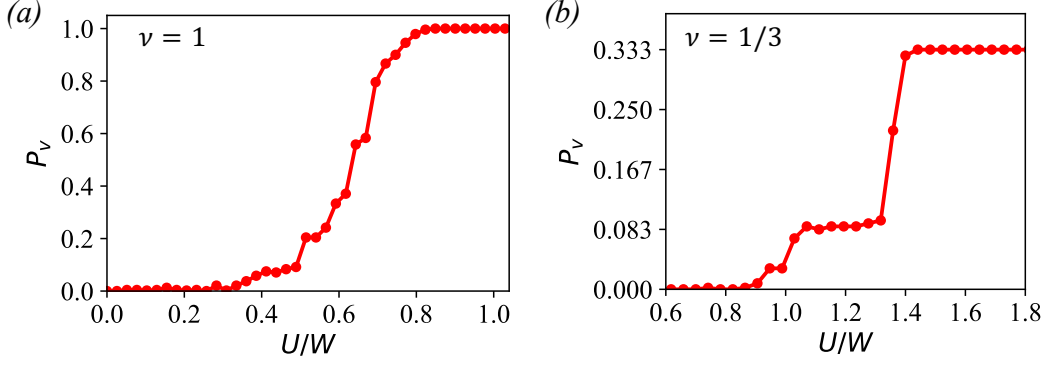


FIG. S1. P_v ($= \sum_{\mathbf{k}} [\Delta_{++}(\mathbf{k}) - \Delta_{--}(\mathbf{k})]$) dependence on interaction (U) for filling ($\nu = 1$) in panel (a) and fractional filling ($\nu = 1/3$) in panel (b). We observe unpolarized metal for smaller U , polarized metal for intermediate U and a valley polarized state for large U .

Here, $h_0(\mathbf{k}) = h_{BM}(\mathbf{k}) - \frac{1}{2}h_{HF}(\Delta_0, \mathbf{k})$ where Δ_0 is the reference density matrix such that $\mathcal{H}_{MF} = h_{BM}$ of symmetry unbroken state when $\Delta_k = \Delta_0$ [S66]. We therefore, choose $\Delta_0 = \begin{pmatrix} \nu/2 & 0 \\ 0 & \nu/2 \end{pmatrix} \forall \mathbf{k}$.

Also, the h_{HF} is given by,

$$h_{HF}^{\tau, \tau'}(\Delta_k, \mathbf{k}) = \frac{U}{2N_{\text{cell}}} \sum_{\mathbf{G}} \nu_{\mathbf{G}} \lambda_{\tau, \mathbf{G}}(\mathbf{k}) \delta_{\tau, \tau'} \sum_{\tau'', \mathbf{k}'} \text{tr}[\lambda_{\tau'', \mathbf{G}}^\dagger(\mathbf{k}') \Delta_{\tau, \tau''}^T(\mathbf{k})] - \frac{U}{2N_{\text{cell}}} \sum_{\mathbf{G}, \mathbf{k}'} \nu_{\mathbf{G}+\mathbf{k}'} \lambda_{\tau, \mathbf{G}+\mathbf{k}'}(\mathbf{k}) \lambda_{\tau', \mathbf{G}+\mathbf{k}'}^\dagger(\mathbf{k}) \Delta_{\tau, \tau'}^T(\mathbf{k} + \mathbf{k}') \quad (\text{S2})$$

In the above equation, the first and second terms are the Hartree and Fock contributions, respectively. Here, N_{cell} is the total area of the MBZ and we have used $\mathbf{q} = \mathbf{G} + \mathbf{k}'$. \mathbf{k}, \mathbf{k}' are momentum vectors in the first Brillouin zone (BZ) and \mathbf{G} is the reciprocal vector connecting different BZs. The matrix, $\lambda_{\tau, \mathbf{q}}(\mathbf{k}) = \lambda_{\tau, \mathbf{G}+\mathbf{k}'}(\mathbf{k})$ contains the form factors for the single particle given by, $\lambda_{\tau, \mathbf{G}+\mathbf{k}'}(\mathbf{k}) = \langle u_{\tau, \mathbf{k}} | u_{\tau, \mathbf{k}+\mathbf{G}+\mathbf{k}'} \rangle$. We also have $\nu_{\mathbf{q}} = \frac{4\pi \tanh(qd)}{q\sqrt{3}a_M}$ for dual-gate screened Coulomb interaction.

For writing the mean-field equation, we use the following condition; a) $\lambda_{+, \mathbf{q}}(\mathbf{k}) = \lambda_{-, -\mathbf{q}}^*(-\mathbf{k})$, and b) the \mathbf{G}_j^{th} component of momentum, $\mathbf{q} = \mathbf{G}_l + \mathbf{k}$ in the l^{th} Moiré Lattice is generated using central BZs as, $|u_{\tau, \mathbf{k}+\mathbf{G}_l}(\mathbf{G}_j)\rangle = |u_{\tau, \mathbf{k}}(\mathbf{G}_j + \mathbf{G}_l)\rangle$, so as to have a consistent gauge.

One can write the new quasiparticle by solving the above equation; $V^\dagger H_{MF} V V^\dagger |\psi\rangle = E_n V^\dagger |\psi\rangle$. One can evaluate the Hamiltonian as $\langle \psi | V V^\dagger H_{MF} V V^\dagger |\psi \rangle = \langle \phi | D | \phi \rangle$ where

$$|\psi(\mathbf{k})\rangle = \begin{pmatrix} C_+(\mathbf{k}) \\ C_-(\mathbf{k}) \end{pmatrix} = V(\mathbf{k}) |\phi(\mathbf{k})\rangle = \begin{pmatrix} u_1(\mathbf{k}) & u_2(\mathbf{k}) \\ v_1(\mathbf{k}) & v_2(\mathbf{k}) \end{pmatrix} \begin{pmatrix} \gamma_1(\mathbf{k}) \\ \gamma_2(\mathbf{k}) \end{pmatrix} \quad (\text{S3})$$

The gap $\Delta_{\tau, \tau'}(\mathbf{k}) = \langle C_\tau^\dagger(\mathbf{k}) C_{\tau'}(\mathbf{k}) \rangle$ has to be written in terms of these new quasiparticles

We now write the gap equation in the new basis,

$$\Delta_{\tau, \tau'}(\mathbf{k}) = \langle C_\tau^\dagger(\mathbf{k}) C_{\tau'}(\mathbf{k}) \rangle = \begin{pmatrix} |u_1(\mathbf{k})|^2 \langle n_{\gamma_1}(\mathbf{k}) \rangle + |u_2(\mathbf{k})|^2 \langle n_{\gamma_2}(\mathbf{k}) \rangle & u_1^*(\mathbf{k}) v_1(\mathbf{k}) \langle n_{\gamma_1}(\mathbf{k}) \rangle + u_2^*(\mathbf{k}) v_2(\mathbf{k}) \langle n_{\gamma_2}(\mathbf{k}) \rangle \\ u_1(\mathbf{k}) v_1^*(\mathbf{k}) \langle n_{\gamma_1}(\mathbf{k}) \rangle + u_2(\mathbf{k}) v_2^*(\mathbf{k}) \langle n_{\gamma_2}(\mathbf{k}) \rangle & |v_1(\mathbf{k})|^2 \langle n_{\gamma_1}(\mathbf{k}) \rangle + |v_2(\mathbf{k})|^2 \langle n_{\gamma_2}(\mathbf{k}) \rangle \end{pmatrix}. \quad (\text{S4})$$

Here $n_{\gamma_m}(\mathbf{k}) = \gamma_m^\dagger(\mathbf{k}) \gamma_m(\mathbf{k})$ Also, filling in the new basis is given by

$$\bar{n} = \sum_{\tau, \mathbf{k}} \langle C_\tau^\dagger(\mathbf{k}) C_\tau(\mathbf{k}) \rangle = \sum_{\mathbf{k}} \text{tr}[\Delta_{\tau, \tau'}] = \sum_{\mathbf{k}} \langle n_{\gamma_1}(\mathbf{k}) \rangle + \langle n_{\gamma_2}(\mathbf{k}) \rangle = \nu \quad (\text{S5})$$

Eqs. S4 and S5 are then solved self-consistently for a fixed filling, until μ and mean field order parameter or all \mathbf{k} converges. But, we use a relatively relaxed condition for convergence, as $\Delta_{\tau, \tau'}(\mathbf{k})$ can have multiple degenerate configurations, therefore, we use $\max(\Delta^n - \Delta^{n+1}) < \text{tolerance limit}$, where $\Delta = \sum_{\mathbf{k}} \Delta_{\tau, \tau'}(\mathbf{k})$. In the numerical simulation, we observe that only diagonal element of $\Delta_{\tau, \tau'}(\mathbf{k})$ are populated whereas the off-diagonal elements are zero, meaning that valley polarized state is the ground state. We define a valley polarization order parameter $P_v = \sum_{\mathbf{k}} [\Delta_{++}(\mathbf{k}) - \Delta_{--}(\mathbf{k})]$.

In Fig. S1, we plot P_v dependence on the interaction (U) for ($\nu = 1$) and fractional ($\nu = 1/3$) fillings using the parameters discussed in the main text and at $\theta = 1.38^\circ$. In the case of filling ($\nu = 1$) shown in Fig. S1 (a), we observe that till around $U = 0.3W$ we have unpolarized metal, *i.e.* equal number of electron in both the valleys. For an intermediate interaction, $0.3W \leq U \leq 0.8W$, we observe partially polarized metal and from $U = 0.8W$ onward the system is fully polarized. Here, W is the bandwidth of the non-interacting bands. The band in one valley is fully occupied and the system is a valley polarized insulator. This behavior is consistent with the results reported for twisted bilayer graphene in the Ref. [S27].

On the other hand, in the case of the fractional filling ($\nu = 1/3$) shown in Fig. S1 (b), we observe the system to be unpolarized metal till $U = 0.85W$. In the $0.85W \leq U \leq 1.4W$ regime, partially polarized metal is observed and finally above, $U = 1.4W$, the system saturates into a completely polarized metal. Note that in this filling fraction, one can only partially fill the lower mean-field band. Hence, the system remains a metal in contrast to the case with $\nu = 1$.

III. Possibility of the Halperin state

Here we argue that it is unfavorable to host the Halperin (m_1, m_2, n_1) states in TMD Moiré superlattice, because of the opposite Chern number in the opposite valleys. For a flat Chern band, a good starting point to understand the physics is the Landau level by neglecting the variation of the Berry curvature and band dispersion. The Chern bands in the \pm valleys in TMD Moiré superlattice can be treated as Landau levels stabilized by opposite effective magnetic field, $\pm B$. The wave function for the Halperin (m_1, m_2, n_1) state is

$$|\Psi_H\rangle = \prod_{i < j} (z_{+i} - z_{+j})^{m_1} (z_{-i} - z_{-j})^{m_2} (z_{+i} - z_{-j})^{n_1} \exp \left[- \sum_{i, \tau = \pm} \frac{1}{4l_B^2} |z_{\tau i}|^2 \right],$$

where $z_{\pm i} = x + iy$ and $l_B = \sqrt{\hbar c / eB}$ is the magnetic length. Introducing composite particle through the flux attachment [S67]

$$\phi_\tau(r) = \exp(i\Theta_\tau) \psi_\tau(r),$$

$$\Theta_+ = m_1 \int dr_2 \theta(r_1 - r_2) \rho_+(r_2) + n_1 \int dr_2 \theta(r_1 - r_2) \rho_-(r_2),$$

$$\Theta_- = m_2 \int dr_2 \theta(r_1 - r_2) \rho_-(r_2) + n_1 \int dr_2 \theta(r_1 - r_2) \rho_+(r_2),$$

where $\theta(r_1 - r_2)$ is the angle between the vector $r_2 - r_1$ and the x axis. $\phi_\tau(r)$ is the composite particle wave function and $\psi_\tau(r)$ is the electron wave function. ρ_τ is the charge density. The effective magnetic experienced by the composite particles are

$$B_{\text{eff},+} = B - \Phi_0 (m_1 \rho_+ + n_1 \rho_-), \quad B_{\text{eff},-} = -B - \Phi_0 (m_2 \rho_- + n_1 \rho_+),$$

with $\Phi_0 = 2\pi\hbar c / e$. It is not possible to make $B_{\text{eff},\pm}$ vanishing for any positive integers (m_1, m_2, n_1). Therefore the Halperin state is generally unflavored in energetics.

IV. Effective theory for the transition between the valley polarized Fermi liquid and fractional Chern insulator

If we take the Landau level point of view by assuming completely flat bands with uniform Berry curvature, we can write down Ginzburg-Landau free energy to describe the phase transition between the Fermi liquid with valley polarization and fractional Chern insulator (FCI), analogous to the case for the transition between the fractional topological insulator and superfluid [S68]. In this consideration, we can think that two valleys experience an opposite magnetic field $B_\tau = \nabla \times a_\tau$. The Lagrangian can be written as

$$\mathcal{L}_\tau = \bar{\psi} (i\partial_t - A_0 - a_{\tau,0}) \psi - \frac{1}{2m_\psi} |(-i\nabla - A - a_\tau)\psi|^2 - V(\psi) + \frac{1}{4\pi m} \epsilon^{\mu\nu\lambda} a_\mu \partial_\nu a_\lambda,$$

$$\mathcal{L}_\phi = \bar{\phi}_\tau (i\partial_t - A_0) \phi_\tau - \frac{1}{2m_\phi} |(-i\nabla - A)\phi_\tau|^2 - \alpha |\phi_\tau|^2 - \frac{\beta}{2} |\phi_\tau|^4,$$

$$\mathcal{L}_\phi = -g|\phi|^2|\psi|^2.$$

Here a_τ is the dynamical gauge field with Chern-Simons term. A is the external electromagnetic gauge fields. ψ describes the FCI condensate and $\phi_\tau = \langle C_\tau^\dagger C_\tau \rangle$ is valley polarization order parameter, and their spatial average value obey $\langle |\psi|^2 + |\phi_\tau|^2 \rangle = \rho_0$ with ρ_0 the electron density. Here m is an integer and we consider electron filling at $1/m$. The term with $g > 0$ describes the repulsion between the FCI condensate and valley polarization condensate. $V(\psi)$ is the potential for the FCI condensate which depends on the electron interaction.

From this construction, it is clear why the Fermi liquid with valley polarization (VP) is favored over the the Fermi liquid with inter-valley coherent state (IVC). In VP, the effective magnetic field due to the valley contrasting Chern band cancels. In \mathcal{L}_ϕ , there is no a_τ gauge field, which is energetically favorable because of energy cost associated with the Meissner screening of a_τ if it is present. Whereas for the IVC, we need to condense $\phi_{\text{IVC}} \sim \langle C_+^\dagger C_- \rangle$. In this case, we will have coupling to the a_τ field: $-\frac{1}{2m_{\text{IVC}}} |(-i\nabla - A - 2a_\tau)\phi_{\text{IVC}}|^2$, which costs energy due to the Meissner effect.

The transition from the Fermi liquid with VP to FCI can be understood as follows. For an intermediate interaction, the Fermi liquid with VP is favored. Due to the repulsion between the FCI and VP condensates, electrons condense into the ϕ_τ channel and the Fermi liquid with VP is stabilized. When the interaction becomes strong, the FCI is favored by the $V(\psi)$ term, and more electrons condense into the FCI state.